

## Chemisorption of hydrogen on the missing-row Pt(110)-(1×2) surface

M. Minca<sup>a</sup>, S. Penner<sup>a</sup>, T. Loerting<sup>a</sup>, A. Menzel<sup>a,\*</sup>, E. Bertel<sup>a</sup>, R. Zucca<sup>b</sup>, and J. Redinger<sup>b</sup>

<sup>a</sup>Institute of Physical Chemistry, University of Innsbruck, Innsbruck, 6020 Austria

<sup>b</sup>Center for Computational Materials Science, Vienna University of Technology, Vienna, 1060 Austria

Chemisorption of hydrogen on the missing-row reconstructed Pt(110)-(1×2) surface has been studied by TPD, quantitative LEED, and DFT calculations. An (atypical) chemisorption site on the outermost close-packed rows with an ideal coverage of 0.5 ML ( $\beta_2$ -state) is found. Adsorption sites on the (111) microfacets are occupied only at higher coverage ( $\beta_1$ -state). After exposures of more than 400 L, the TPD spectra clearly reveal the controversially discussed  $\alpha$ -state. In the same coverage range, an intense 1×4 superstructure becomes visible at LEED energies around 50 eV. The saturation coverage for chemisorption at  $T = 120$  K is 33% higher than assumed previously.

**KEY WORDS:** hydrogen chemisorption; transition metal surfaces; surface reconstruction; surface relaxation; desorption.

The study of the interaction of hydrogen with transition metal surfaces is of fundamental importance. For example, hydrogen plays a central role in a multitude of technologically important catalytic reactions that occur on transition metal surfaces, such as hydrocarbon processing, hydrogenolysis and CO hydrogenation reactions [1]. Other topics of technological interest include hydrogen storage and the embrittlement of materials by hydrogen. More specifically, the H/Pt(110) surface is used as a model system for the behavior of Pt particles in H fuel cells [2,3] and for the design and characterization of 1-dimensional systems on surfaces [4–8].

Recently, we reported an atypical bonding geometry of the so-called  $\beta_2$ -state at a coverage of 0.5 hydrogen atoms per 1×1 unit cell (0.5 ML) [9]: Contrary to the general expectation [10,11] and to proposals specific to the Pt(110) surface [12–15], hydrogen adsorbs in the low coordinated short bridge site on top of the outermost platinum rows. The current paper includes both, the former low coverage results and additionally experimental and theoretical investigations for higher coverages up to saturation. New details on the energetics of the low coverage  $\beta_2$  phase as obtained from DFT calculations are given. As to the saturation coverage, we present clear evidence for a higher value than assumed previously [12]. The TPD spectra show a high-temperature shoulder and the  $\alpha$ -state, an autocatalytic desorption feature similar to H on Ni(110) [11]. In the coverage range of the  $\alpha$ -state, LEED shows the formation of an intense (1×4) structure. Interestingly, the additional spots can only be seen at low primary energies. This parallels findings on Ni(110), where at low temperatures and high coverages a

doubling of the periodicity—most likely a pairing row reconstruction (see Ref. [16] and references therein)—is observed [11].

The experiments were carried out in a UHV system with a base pressure of  $5 \times 10^{-11}$  mbar. The Pt(110) crystal was cut and polished to a precision of  $< 0.1^\circ$ . The crystal was mounted on a five-axis manipulator with facilities for electron bombardment ( $T_{\max} = 1100$  K) and liquid-N<sub>2</sub> cooling ( $T_{\min} = 120$  K). Sputtering with Ar, annealing to 1020 K and heating in oxygen has been used to initially clean the sample. Prior to each measurement, residual carbon was eliminated by 3 cycles of 3 L O<sub>2</sub> adsorption at 130 K (saturation) and subsequent flash desorption (3 K/s) to 920 K. Hydrogen or deuterium were adsorbed at crystal temperatures of 130 K by backfilling the chamber. The exposure given in Langmuir is not calibrated and not corrected for sensitivity factors. The coverage in monolayers (ML) is referred to the adsorbate atom density on a (1×1) unit cell of the—unreconstructed—fcc(110) surface, thus 1 ML amounts to one adsorbate atom per  $1.08 \times 10^{-15}$  cm<sup>2</sup> or  $0.92 \times 10^{+15}$  atoms/cm<sup>2</sup>. Heating rates during temperature programmed desorption (TPD) were 3 K/s if not mentioned otherwise. LEED data have been taken with a CCD camera upon varying the energy (LEED-I/V), temperature, or exposure. Details on the evaluation of the LEED-I/V curves can be found in Ref. [9].

For the density-functional theory (DFT) calculations the Vienna ab-initio simulation Package (VASP) [17] has been used within the generalized gradient approximation (GGA) [18]. All calculated geometric values given have been scaled according to the ratio of the theoretical to experimental bulk lattice constant (3.98 vs. 3.92 Å). Repeated slabs of 11 Pt layers with an ad-layer of H atoms on the missing Pt-row side and a p(1×1) Pt termination on the other side were separated by a 12 Å thick vacuum layer. All layers were relaxed and an

\* To whom correspondence should be addressed.  
E-mail: Alexander.Menzel@uibk.ac.at

energy cutoff of 250 eV and a  $8 \times 8 \times 1$  Monkhorst-Pack type  $k$ -point mesh was sufficiently accurate for the present purposes. The values of the adsorption energies are given per hydrogen atom with respect to its binding energy in the  $H_2$  molecule. A well known inconvenience of GGA is its poorer performance for atom and molecule as compared to substrate or adsorbate system. In order to avoid systematic errors in the DFT adsorption energies, our GGA energies are taken to be the experimental values [19]  $E_H^{\text{at}} = 13.60$  eV for the atom and  $E_{H_2}^{\text{d}} = 4.75$  eV for the dissociation energy of the  $H_2$  molecule, leading to a reduction of the GGA adsorption energies by 90 meV.

The TPD spectra obtained in the present study (see figure 1) qualitatively show all features of data sets published previously by other groups [2,12,13,20]. The well known  $\beta_2$  and  $\beta_1$  states [12,13], and—at exposures above 400 L—the additional  $\alpha$ -state [2,20] are reproduced. The coverage versus exposure curve (see figure 2) derived from the data set in figure 1 is virtually the same as has been found in ref. [12] for exposures up to 175 L. Our data indicate, however, that saturation under these conditions is only reached after exposures exceeding 2000–5000 L. In figure 1, the open symbols represent a tentative principal component analysis of the TPD at saturation coverage. For separating the components, the TPD spectra at 0.67 L and 133 L have been assumed to be solely due to the  $\beta_2$  and the sum of  $\beta_2$  and  $\beta_1$  state, respectively. Consequently, the contributions of the  $\beta_1$  and the  $\alpha$  state are represented by the difference of the TPD spectra at 133 L minus 0.67 L and 10000 L minus 133 L, respectively. The partition is of course based on these assumptions and should not be taken too seriously. It is merely intended to show that the TPD at saturation

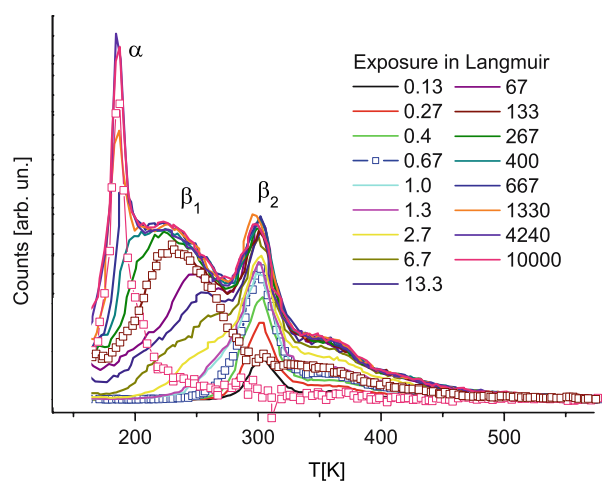


Figure 1. TPD spectra for  $D_2$ . The exposure has been varied from 0.13 to 10000 L. Open symbols represent the principal components of the TPD spectrum at saturation (10000 L) divided into areas due to the  $\alpha$ -state (pink symbols, integrated area 27% of total), the  $\beta_1$ -state (brown, 51%), and the  $\beta_2$ -state (blue, 22%). See text for a description of the decomposition.

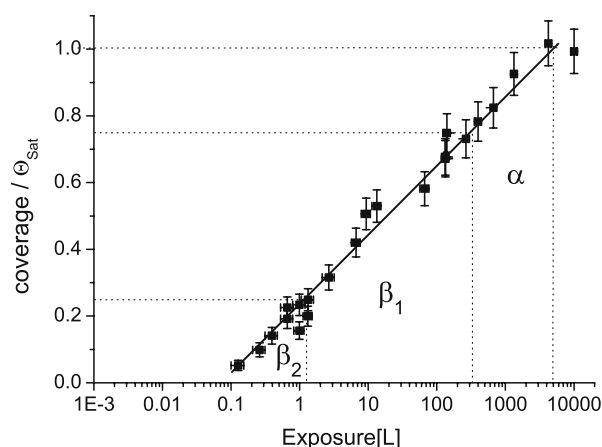


Figure 2. The coverage-exposure relationship for the full data set on  $D_2$  shown (partly) in figure 1. The solid line is drawn to emphasize the apparent logarithmic dependence, dotted lines represent the partition of coverage into the three different states with an assumed ratio of 1:2:1.

is consistent with a relative ratio of 1:2:1 for  $\beta_2$ : $\beta_1$ : $\alpha$  within the error bars of the experiment. This partition agrees well with (i) the approximate ratio of 1:2 for  $\beta_2$ : $\beta_1$  which has been found earlier [12], (ii) with a CO coadsorption experiment blocking the  $\beta_2$  state (see below, figure 6), and (iii) with our DFT calculations (see below, figure 8). According to the calibration of absolute coverage [12] and following the conclusions drawn in Ref. [12], this indicates a saturation coverage of 2 H atoms per  $(1 \times 1)$  unit cell (2 ML) or 4 H atoms per missing-row  $(1 \times 2)$  unit cell. We caution here, that for fcc(110) surfaces, the coverage in ML is usually referred to the  $(1 \times 1)$  unit cell of the unreconstructed surface which contains one substrate atom on the outermost row. However, these surfaces are quite “open”, the second and third layer atoms are still fairly exposed. Here, in the case of a missing-row reconstruction, the  $(1 \times 2)$  unit cell contains four more or less exposed Pt atoms. The saturation coverage of 4 H atoms per  $(1 \times 2)$  unit cell found in our work thus corresponds to one hydrogen atom per “exposed” Pt atom (see figure 8). This saturation coverage is roughly a factor of 4/3 higher than was assumed previously [12]. Interestingly, the overall coverage seems to be proportional to the logarithm of the exposure. TPD spectra of hydrogen yield the same results, experimentally indistinguishable from the deuterium data.

Note that the TPD spectra in figure 1 also reveal a weak high temperature tail or shoulder at around 350 K as has been found in one of the earlier investigations [2]. Judging from figure 1, this feature seems to grow with both,  $\beta_2$  and  $\beta_1$  state, which is one reason for the above partition to be somewhat ambiguous. In order to show that this shoulder is not due to an experimental artefact, we varied experimental parameters like heating rate (1–10 K/s), sample-spectrometer distance and alignment. The shoulder could be observed in all TPD spectra and,

additionally, seems not to be induced by defects: In an attempt to reveal the influence of defects qualitatively, we recorded some TPD spectra after soft sputtering of the surface. As can be seen in figure 3, the defects from sputtering induce a broadening of the peaks in the TPD spectrum. The shoulder is not observable for surfaces with higher defect-density which indicates some broadening as well, but no increase. Another indication for the shoulder being a genuine feature of the surface is the observation of this feature in a CO coadsorption experiment (see figure 6). Furthermore, the high temperature feature is certainly not due to just another high binding energy site, since it cannot be populated independently for low exposures (see figure 1). Effects of desorption kinetics, mediated e.g. by a substantial temperature and coverage dependent substrate response (see below), and the strong anisotropy of the surface complicate the interpretation of TPD spectra, of course. We note that our crystal has an extremely low miscut, a parameter which could also distinguish the various earlier experiments [2,12–15,20]. Lower heating rates than 1 K/s would be interesting, but were not feasible with our current experimental setup. With respect to the dependence of the sticking coefficient on defect density, we note that the coverage at exposures of 15 L increases from roughly 45% of saturation coverage on the defect-free surface to 60% after sputtering. We conclude—in agreement with earlier suggestions [20]—that the extremely small sticking coefficient at higher coverage depends critically on topological details like step and kink density. It is well known that even a comparably small miscut of the crystal leads to the so-called fish scale pattern of the Pt(110) surface [21]. This fact may resolve the controversy about the  $\alpha$ -state: Whereas in some of the earlier experiments [12,13] the high exposures needed for occupation of the  $\alpha$ -state have not been applied, a higher sticking coefficient at higher coverages

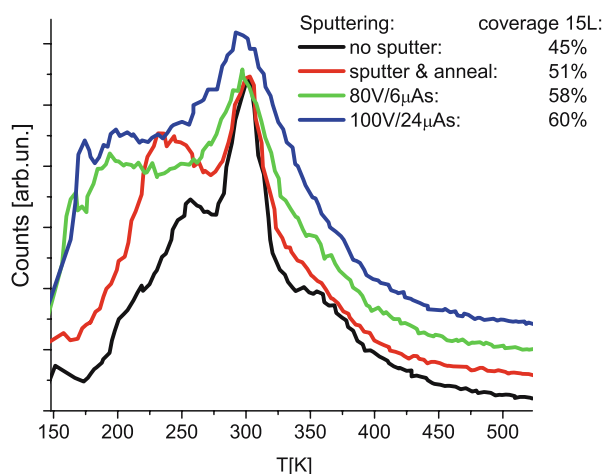


Figure 3 TPD spectra of  $D_2$  after soft sputtering the surface with slow argon (80–100 eV) ions before adsorption. For better comparison, the spectra are offset by a constant.

(see figures 6 and 2 in Refs. [2,20], respectively) allowed the detection of the  $\alpha$ -state at exposures below 60 L. For a general overview, we first repeat the main findings for the  $\beta_2$  state (low coverage) as already published (figure 4, see [9]). Then we give more and yet unpublished details on the DFT geometries and energetics at low coverage (see table 1) and discuss the experiments and calculation for the  $\beta_1$  and  $\alpha$ -states at higher coverage.

Figure 4 summarizes the main conclusions drawn from the LEED-I/V experiments on the bonding geometry and H-induced changes of the  $\beta_2$ -state at 0.5 ML coverage. For details, the reader is referred to Ref. [9]. According to the I/V-LEED analysis, the most important change upon hydrogen adsorption is the derelaxation in the first interlayer spacing  $d_{12}$  (see figure 4): The interlayer spacing in (110) direction in the bulk, for the clean and for the  $\beta_2$ -H/Pt(110) is  $d_{12}(\text{bulk}) = 1.38 \text{ \AA}$ ,  $d_{12}(\text{clean}) = 1.15 \text{ \AA}$ , and  $d_{12}(\beta_2\text{-H}) = 1.25 \text{ \AA}$ , respectively. Thus, the derelaxation amounts to 0.10  $\text{\AA}$  with respect to the relaxed clean surface geometry. The significant buckling in the third layer and the spacing of the inner layers are roughly constant. The bonding geometry can be determined by a comparison of the result of our LEED experiment with a Helium atom scattering (HAS) experiment [15]. The change in corrugation upon hydrogen adsorption as measured in the HAS experiment alone (+0.5  $\text{\AA}$ ) is consistent with a subsurface site or a site on the outermost row [15]. Both experiments are complementary in the sense that LEED is sensitive to the Pt atom positions whereas HAS is determined by the corrugation of the electron density far above the surface. Figure 4 shows a schematic representation of expected experimental results in case of a subsurface site (left) or in case of an adsorption site on the outermost row. This picture can be utilized to experimentally determine the adsorption site of hydrogen: The change in corrugation upon hydrogen adsorption amounts to +0.1  $\text{\AA}$  in LEED and to +0.5  $\text{\AA}$  in HAS [15]. The combined results of both experiments are only compatible with an adsorption site above the outermost row (figure 4, right).

This conclusion is supported by our DFT calculation, which shows that octahedral and tetrahedral subsurface sites below the outermost row are unstable against molecular desorption. According to the calculation, the lowest-energy site is the short bridge site on the outermost row. Generally, the calculated energies support the conclusions drawn from figure 4, but the calculated interlayer spacing  $d_{12} = 1.32 \text{ \AA}$  for a perfect  $\beta_2$ -H/Pt(110) phase at 0.5 ML, is slightly bigger than the experimental  $d_{12} = 1.25 \text{ \AA}$ . Since the calculation does not include finite temperature effects, we calculated the dependency of the Pt relaxation and the chemisorption energy on the H atom position. Table 1, not published in Ref. [9], shows the calculated interlayer spacings and

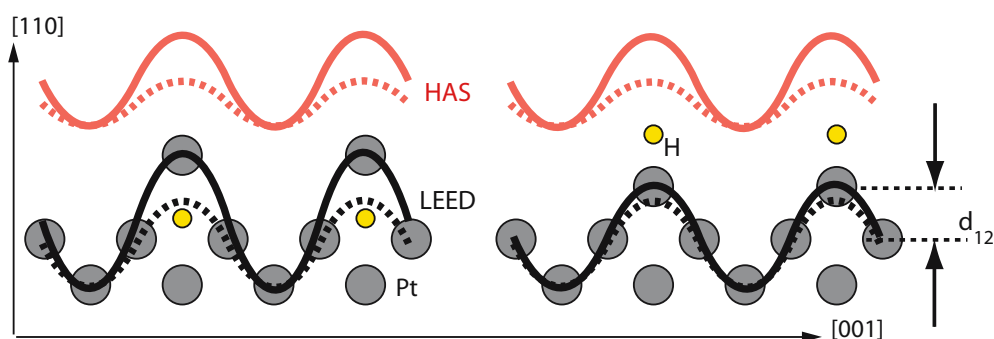


Figure 4. Side view of the surface,  $d_{12}$  is the first interlayer spacing in (110) direction. Schematic representation of the expected experimental corrugation (HAS, red curves; LEED, black curves) on the hydrogen modified Pt(110) surface. The left part of the figure shows the corrugations in case of hydrogen atoms (yellow) adsorbing below the outermost Pt row, whereas on the right the case of hydrogen adsorbing above the outermost row is shown. The LEED-corrugation follows essentially the Pt atom positions (total electron density), whereas HAS detects profiles of (low) constant charge density (Pauli repulsion). The smaller corrugation of the clean surface is represented by the dotted lines. The right case is the one found experimentally.

energies depending on the 33 different H positions (see figure 5) on the surface.

Generally, the table shows that the positions with highest binding energies are located in the vicinity of the rim and correlate with the biggest interlayer spacings  $d_{12}$ . Adsorption in the trough is most unfavoured and leads to the lowest  $d_{12}$ . The energies and geometries as given in table 1 enable an estimate of the potential landscape and to picture the diffusion and vibrational amplitudes of the hydrogen atom in correlation with  $d_{12}$ . The potential in the direction vertical to the bridge site (lower row in table 1 and line b in figure 5) is obviously very flat, so the vibrational amplitude will be enhanced perpendicular to the outermost Pt row. The average interlayer spacing will decrease due to this vibrational motion, which suggests thermal motion as the source for the deviation of experimental and theoretical values in case of the  $\beta_2$  state. The overall potential landscape indicates a strongly anisotropic diffusion which proceeds most easily along the Pt rows. Diffusion paths on the rim of the outermost row or on the facet near to the rim have similar barriers. The highest barrier is encountered in the direction perpendicular to the Pt rows, which is in contrast to the findings for H/Ni(110) [16].

Our results confirm an HREELS experiment of H/Pt(110) [14] indicating a 2-fold bridge site at low coverage.

The small induced work function change [12,13] indicates a rather covalent bonding within the present model. In comparison, the most stable bonding site of H on Ni(110) and Pd(110) is the fcc pseudo-threefold site at the (111) microfacets of the (110) surface [16,22]. We attribute the peculiar bonding characteristics of H on Pt to a strong covalent interaction with the Pt d-orbitals. As we have suggested earlier for Br/Pt(110) [23] and also in a comparative study of CO-bonding on the transition metal surfaces [24], these bonding characteristics result from the relativistic contraction of the s-orbitals and the concomitant d-shell expansion.

Independent support for the short bridge site as the preferred adsorption site can be found by preadsorption of CO. As shown in figure 6, the  $\beta_2$ -state in TPD is completely quenched by preadsorption of CO (exposure 0.66 L), whereas the  $\beta_1$ -state and the shoulder at higher temperatures are not affected. Since CO is known to adsorb on top of the outermost Pt rows [25], the quenching of the  $\beta_2$ -state supports an adsorption site for hydrogen on the outermost row, too. As has been mentioned above, the CO coadsorption experiment can also be analyzed with respect to the relative coverage of the  $\beta_2$  state. Assuming that all  $\beta_2$  adsorption sites have been blocked with CO, the difference curve in figure 6 should correspond to the contribution of the  $\beta_2$  state.

Table 1

Theoretical interlayer spacing (upper value, in Å) and adsorption energies (lower value, in meV) relative to the short bridge site (absolute chemisorption energy  $E_{sb} = -0.489$  eV per H-atom) of the hydrogen-modified  $\beta_2$ -H/Pt(110) ( $1 \times 2$ ) surface at a coverage of 0.25 ML. Labels on columns (in percent of unit cell) and rows (top, tb, and bridge) refer to the H positions on the grid shown in figure 5.

[1 $\bar{1}$ 0]	Position in [001]										
	0	5	10	15	20	25	30	35	40	45	50
Top	1.195	1.203	1.189	1.185	1.098	1.086	1.086	1.086	1.110	1.115	1.124
	116	118	125	163	190	159	165	186	260	439	559
tb	1.200	1.198	1.203	1.149	1.107	1.099	1.094	1.089	1.077	1.108	1.064
	169	173	178	213	125	193	202	185	236	333	415
Bridge	1.224	1.200	1.169	1.134	1.121	1.091	1.083	1.090	1.086	1.050	0.949
	0	19	69	74	164	187	124	82	120	233	276

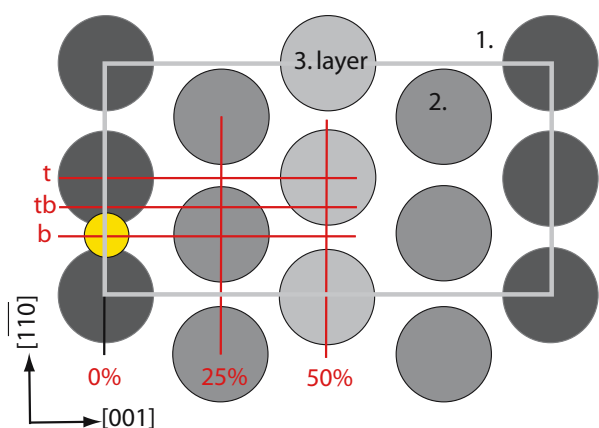


Figure 5. Top view of the missing-row reconstructed H/Pt(110) surface. Dark, middle and light grey circles represent first, second, and third layer Pt atoms. For the DFT calculation at 0.25 ML, the H atom (yellow) has been fixed on 33 points of a grid (red) parallel to the surface. The  $2 \times 2$  unit cell was mapped using three grid positions in  $[1\bar{1}0]$  direction (on top (t), bridge (b) and in between (tb)), and eleven grid positions in  $[001]$  direction (in steps of 5%). See table 1 for results.

An integration of the curve yields 20% of saturation coverage, which is -taking into account the crudeness of the approximation- agreeing reasonably well with the results discussed above. Judging from figure 6, the higher temperature feature at 350 K contains both, a tail and a shoulder related to the  $\beta_2$  and the  $\beta_1$ -state, supporting the partition as shown in figure 1.

As has been discussed above, our TPD experiments—in agreement with some of the previous investigations [2, 20]—show clear evidence for the so-called  $\alpha$ -state at the highest coverages. In the following, we show that the development of the sharp peak of the  $\alpha$ -state in TPD is accompanied by a new  $(1 \times 4)$  superstructure induced by these high coverages of hydrogen.

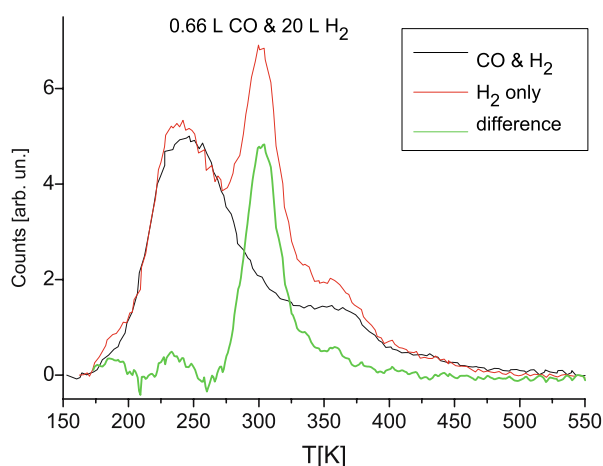


Figure 6. TPD spectra of  $H_2$  with and without preadsorption of CO. The difference (green) of the TPD spectra of the H-covered surface (red) and the CO+H covered surface (black) is equivalent to the  $\beta_2$ -state.

Figure 7 shows the LEED patterns observed for three different coverages. At low LEED energies (49 eV), the  $(1 \times 2)$  periodicity of the missing-row reconstruction remains unchanged up to exposures of 380 L. In a TPD of the same surface, the sharp peak related to the  $\alpha$ -state is not yet observed, the coverage is evaluated to be about  $0.84(\pm 4)\%$  of saturation. At higher exposures (840 and 1430 L), a very intense  $(1 \times 4)$  spot becomes visible in LEED and the sharp  $\alpha$ -state starts to develop in TPD (coverage  $0.90(\pm 3)\%$  to  $0.96(\pm 4)\%$ ). The LEED intensity decreases sharply for exposures higher than 2000 L (coverage  $98(\pm 2)\%$ ), but is still clearly visible for highest exposures (7100 L, saturation coverage), whereas the  $\alpha$ -state in TPD increases up to saturation. Since the  $(1 \times 4)$  spots in LEED at 49 eV are almost as intense as the  $(1 \times 1)$  spots, it seems unreasonable to assign the  $(1 \times 4)$  superstructure solely to a new periodicity within the overlayer of the (weakly scattering  $[1\bar{1}])$  hydrogen atoms. Instead, the Pt(110) substrate atoms are involved in this reconstruction and the local cluster of rearranged Pt atoms around the additional  $\alpha$ -state H atom is responsible for the diffraction spots. The local rearrangement as calculated by DFT is essentially a horizontal shift (see figure 8e) of the second layer Pt atoms towards the (red)  $\alpha$ -state H-atom. Based on preliminary STM data, we speculate that a pairing row reconstruction is responsible for the  $1 \times 4$  overstructure. The analysis of I/V-LEED experiments did not yield a conclusive result on the geometry, since the data-base is severely restricted by the small energy range where the  $1 \times 4$  spots are clearly visible. A pairing row reconstruction has also been observed in the case of H/Ni(110) (see e.g. [16] and references therein) and is suggested to be one of the competing phases for the H induced  $(1 \times 2)$  overstructure of H/Pd(110). Surprisingly, however, a possible row pairing in the present case would involve rows which are separated by almost 0.8 nm due to the missing row reconstruction, and would indicate a rather long range interaction induced by the hydrogen.

In order to complete the picture of H chemisorption on Pt(110), we calculated several geometries for 1.5 ML ( $\beta_1$ -state) and 2.0 ML ( $\alpha$ -state) hydrogen on the surface. Figure 8 summarizes the results of our DFT calculations. The three different adsorption states ( $\beta_2$ ,  $\beta_1$  and  $\alpha$ ) identified in the TPD spectra are confirmed by the calculations as well as the suggested saturation coverage partition of 1:2:1. The rather large difference in adsorption energies between the  $\beta_2$ -hydrogen (figure 8a, white circles) and  $\beta_1$  state (figure 8b, green circles) explains the predominant filling of the former at low coverages. For the  $\beta_1$  state the situation is different, as filling the 111 pseudo-facets (figure 8c) is only by 22 meV less stable, suggesting considerable disorder upon heating, and making desorption from different sites possible (see also figure 8d), consistent with a broader TPD signal. The first interlayer spacing

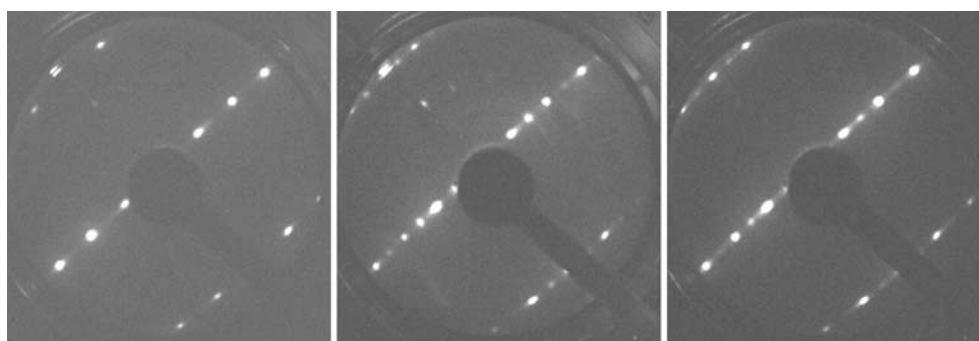


Figure 7. LEED diffraction patterns at  $T = 130$  K and 49 eV electron energy after  $D_2$  exposures of 380 L (left,  $1 \times 2$  pattern), 840 L (middle,  $1 \times 4$  pattern), and 7100 L (right, weaker  $1 \times 4$  pattern).

( $d_{12}(1.5 \text{ ML}) = 1.23 \text{ \AA}$ ) is again less than in the  $\beta_2$ -state ( $d_{12}(0.5 \text{ ML}) = 1.32 \text{ \AA}$ ). This is consistent with the HAS experiment by Kirsten *et al.* [15], where a lowering of the corrugation at higher coverage has been found. The occupation of the  $\beta_1$  state with two additional H atoms left and right of the missing row is plausible, since the distance between the H atoms is large enough to prevent a strong repulsion, and as shown in table 1, the trough states are not favorable. The latter fact is also evident from figure 8e, the  $\alpha$ -state, where the additional H trough atom (red circle) induces a significant distortion of the Pt 111-like microfacets, leading to a row pairing of  $0.4 \text{ \AA}$  in the second Pt layer. In order to

reduce the H–H repulsion on the 111 microfacets, the additional H atom has to be put in the troughs, which according to Table I costs 276 meV as compared with H in the  $\beta_2$ -state for a single atom. This is remarkably close to the adsorption energy difference for the additional  $\alpha$ -H with respect to the full  $\beta_2$ -H-layer ( $489 - 192 = 297 \text{ meV}$ ) as moving the  $\beta_1$ -H to the microfacets is easily accomplished, which makes repulsion between the  $\alpha$ -H and the  $\beta_1$ -H no longer an issue. Now, that the microfacets and trough sites are occupied, adding additional H (blue circles) strongly decreases the H–H distance as seen in figure 8f, which makes further atomic adsorption unlikely.

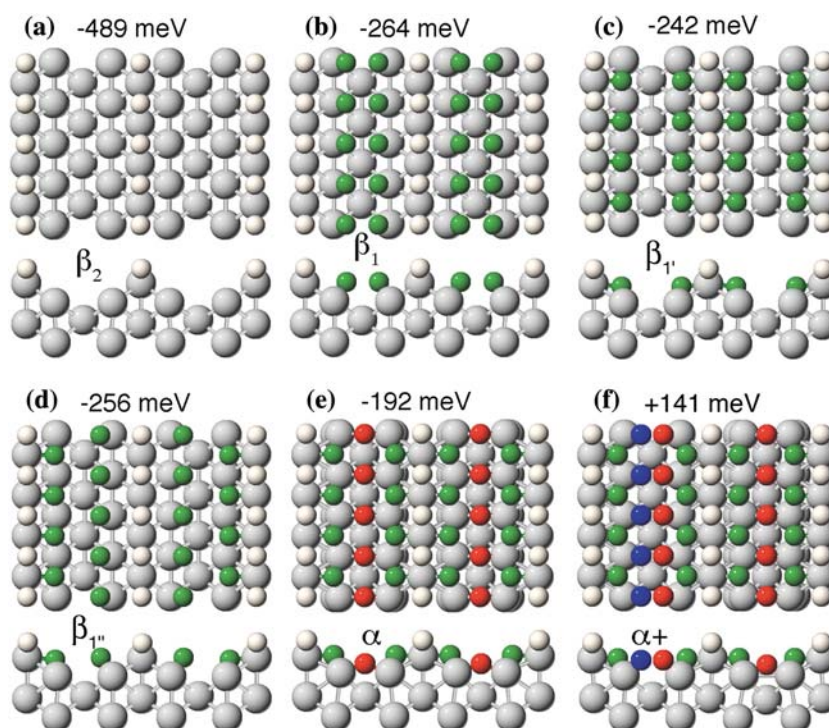


Figure 8. DFT adsorption energies for H on  $(1 \times 2)$  Pt(110). Numerical values refer to the adsorption energy change per additional hydrogen atom (white, green, red, blue) in the specific adsorption site ( $\beta_2$ ,  $\beta_1$ ,  $\alpha$ ,  $\alpha +$ ) and are given with respect to its binding energy in the  $H_2$  molecule. The saturation coverage found in this work corresponds to full occupation of the  $\alpha$  state as shown in e). There are 4 hydrogen atoms per  $(1 \times 2)$  unit cell which translates to a nominal coverage of 2 ML.

In conclusion, the present study reveals an atypical binding site for H/Pt(110) at low coverage ( $\beta_2$ -state), namely the low-coordinated short bridge site on the outermost row of the missing-row reconstructed substrate. Furthermore, a substantial derelaxation of the Pt(110) substrate and a strong coupling of the Pt lattice relaxation to the H atom position has been found. At higher coverages ( $\beta_1$ -state), sites on the (111) microfacets become occupied. For exposures higher than approximately 400 L the  $\alpha$ -state is evident in the TPD experiments. The relative weight of the three states is near to 1:2:1 and the absolute coverage is compatible to 1:2:1 H atoms per  $1 \times 2$  unit cell. Thus, the saturation coverage is higher than previously assumed and amounts to 4 H atoms per  $(1 \times 2)$  unit cell. At low LEED energies, a distinct  $(1 \times 4)$  pattern develops in the coverage range of the  $\alpha$ -state.

### Acknowledgment

Support of this work by the Austrian Science Fund is gratefully acknowledged.

### References

- [1] M. Fuchs, B. Jenewein, S. Penner, K. Hayek, G. Rupprechter, D. Wang, R. Schlögl, J. Calvino and S. Bernal, *Appl. Cat. A* 294 (2005) 279.
- [2] C. Lu and R.I. Masel, *J. Phys. Chem. B* 105 (2001) 9793.
- [3] W. Chrzanowski and A. Wieckowski, *Langmuir* 14 (1998) 1967.
- [4] P. Segovia, D. Purdie, M. Hengsberger and Y. Baer, *Nature* 402 (1999) 504.
- [5] A. Mugarza, A. Mascaraque, V. Prez-Dieste, V. Repain, S. Rousset, F.J.G. de Abajo and J.E. Ortega, *Phys. Rev. Lett.* 87 (2001) 107601/1.
- [6] N. Nilius, T.M. Wallis and W. Ho, *Science* 297 (2002) 1853.
- [7] W. Widdra, P. Trischberger and J. Henk, *Phys. Rev. B* 60 (1999) R5161.
- [8] W. Widdra, *Appl. Phys. A* 72 (2001) 395.
- [9] Z. Zhang, M. Minca, C. Deisl, T. Loerting, A. Menzel, E. Bertel, R. Zucca and J. Redinger, *Phys. Rev. B* 70 (2004) 121401.
- [10] G. Burns, *Solid State Physics* (Academic Press, New York, 1985).
- [11] K. Christmann, *Surf. Sci. Rep.* 9 (1988) 1.
- [12] J.R. Engstrom, W. Tsai and W.H. Weinberg, *J. Chem. Phys.* 87 (1987) 3104.
- [13] C.S. Shern, *Surf. Sci.* 264 (1992) 171.
- [14] W. Stenzel, S.A. Jahnke, Y. Song and H. Conrad, *Progress in Surf. Sci.* 35 (1991) 159.
- [15] E. Kirsten, G. Parschau, W. Stocker and K.H. Rieder, *Surf. Sci.* 231 (1990) L183.
- [16] G. Kresse and J. Hafner, *Surf. Sci.* 459 (2000) 287.
- [17] G. Kresse and J. Furthmüller, *Phys. Rev. B* 54 (1996) 11169, see also URL: <http://cms.mpi.univie.ac.at/vasp>; G. Kresse and D. Joubert, *Phys. Rev. B* 59 (1999) 1758.
- [18] Y. Wang and J. Perdew, *Phys. Rev. B* 44 (1991) 13298.
- [19] S. Wilke, D. Hennig and R. Löber, *Phys. Rev. B* 50 (1994) 2548.
- [20] G. Anger, H.F. Berger, M. Luger, A.W.S. Feistritz and K.D. Rendulic, *Surf. Sci.* 219 (1989) L583.
- [21] P. Hanesch and E. Bertel, *Phys. Rev. Lett.* 79 (1997) 1523.
- [22] W. Dong, V. Ledentu, P. Sautet, E. Eichler and J. Hafner, *Surf. Sci.* 411 (1998) 123.
- [23] A. Menzel, K. Swamy, R. Beer, P. Hanesch, E. Bertel and U. Birkenheuer, *Surf. Sci.* 454–456 (2000) 88.
- [24] E. Bertel, N. Memmel, G. Rangelov and U. Bischler, *Chem. Phys.* 177 (1993) 337.
- [25] R.K. Sharma, W.A. Brown and D.A. King, *Surf. Sci.* 414 (1998) 68.